Innovative: International Multi-disciplinary Journal of Applied Technology
(ISSN 2995-486X) VOLUME 04 ISSUE 08, 2026

A SIMULATOR INDEPENDENT DYNAMIC EFFECTIVENESS-NTU MODEL FOR HEAT-EXCHANGER PERFORMANCE PREDICTION UNDER FLOW, TEMPERATURE, AND FOULING DEPENDENT OPERATION

Hassanin M. Ali
Department of Chemical Engineering, College of Engineering, University of Babylon, Babil 51001, Iraq
E-mail: eng.hassanin.mehsin@uobabylon.edu.iq

Abstract:
Fouling is the dominant cause of the progressive loss of thermal duty in industrial heat exchangers, yet the design and monitoring of these units still rely largely on constant fouling factors that ignore the dependence of deposition on flow rate and surface temperature. This work develops a self-contained, simulator-independent mathematical model that couples the steady-flow energy balance, the logarithmic-mean-temperature-difference (LMTD) relation and the effectiveness–number-of-transfer-units (ε–NTU) formulation to an asymptotic, Kern–Seaton-type fouling law whose deposition and removal terms are written as explicit functions of tube velocity and film temperature. The overall heat-transfer coefficient, the effectiveness and the duty are advanced in time by integrating a single ordinary differential equation for the fouling resistance, with the thermal field solved quasi-steadily at each instant. Closed-form normalized sensitivity coefficients are derived for the effectiveness, the duty and the overall coefficient with respect to NTU, mass flow rate, inlet temperature difference and fouling resistance, and a dimensionless fouling-degradation number $\Theta = U_c R_f^*$ is introduced to collapse the asymptotic performance loss onto a single group. The framework is verified against the exact ε–NTU/LMTD duty identity and against the analytical solution of the fouling law, and is then exercised on a thermodynamically consistent counterflow shell-and-tube case study. At the design velocity the model predicts a 20% reduction in the overall coefficient, a 10.7% loss of duty and a 30-day fouling time constant, and it reproduces the experimentally reported inverse-square dependence of that time constant on velocity. An uncertainty analysis quantifies the amplification of measurement error near a close temperature approach. The resulting model is transparent, computationally trivial and readily embedded in performance-monitoring and cleaning-schedule tools.

Keywords: Heat-exchanger performance; Fouling dynamics; Effectiveness–NTU method; Logarithmic mean temperature difference; Asymptotic fouling resistance; Analytical sensitivity analysis; Thermal degradation; Cleaning-schedule optimization

Introduction

Heat exchangers recover a large fraction of the energy reused in crude-oil refining, petrochemicals, power generation and food processing, so their thermal performance bears directly on plant energy efficiency, operating cost and greenhouse-gas emissions. That performance is not fixed. Deposits accumulate on the transfer surface, add a thermal resistance that grows with time, and progressively starve the exchanger of duty. In refinery pre-heat trains this fouling penalty is paid as additional furnace firing, lost throughput and unscheduled shutdowns [1], [2].

In spite of the economic importance of this issue, conventional design still considers fouling on a single immutable parameter: an average value derived from tabulated data and applied just once to the clean overall coefficient in the design phase [3]. There are two problems with this lumped, steady-state device. It assumes fouling is a fixed allowance, not an evolving process so the exchanger is either clean or fully fouled with no in-between consequences. More seriously, it ignores the parameters that really control deposition local surface temperature and wall shear stress, and so flow rate [4], [5]. Identical geometry of two exchangers which work with different velocities or film temperatures foul as fouling at different rates and settling at different asymptotic states, yet the fixed factor gives them the same number.

The specific thermal relations that were necessary to do better have long been established. The methods based on the steady-flow energy balance, both log-mean-temperature-difference (LMTD) and effectiveness–number-of-transfer-units (ε–NTU), provide exact and complete descriptions of the thermal performance of an exchanger with a given overall coefficient [6], [7],[8]. The only difference at this stage is which variables are considered known, the ε–NTU form is the obvious choice for an installed unit, whose area must be fixed and whose outlet temperatures (and thus duty) fall as the coefficient deteriorates, just what fouling is. But both approaches, however, assume a constant coefficient and do not discuss its evolution with time. Time-varying versions of the ε–NTU concept have been developed for step changes in inlet conditions [9], and for units undergoing discharge of matter [10], both confirming that the framework extends into the time domain, but neither addresses fouling, which occurs at a much slower time scale than the thermal transients (order of minutes) we consider here (weeks to months), so the results from our transient treatment can be assumed instantaneous and well-approximated by quasi-steady heat exchanger analysis.

Epstein organized fouling by the style of the mechanism and associated sequences of deposition and removal events, two attributes that reappear in every quantitative model: net growth is equal to a deposition term minus a removal term, with both dependent on local surface temperature and shear. The earliest and still most influential statement of this balance has been given by Kern and Seaton writing the net rate as a constant deposition flux minus a removal term proportional to the amount accumulated [11], integration yielding the characteristic asymptotic approach to a plateau which is still for many observers the default description under steady conditions [12]. Ebert and Panchal incorporated a complementary threshold for the chemical-reaction fouling of crude oil [13], and subsequent refinements confirm that dep increases with surface temperature via an Arrhenius factor while removal compliance increases with wall shear, and velocity [14].

The current state of the art consists of distributed first-principles models building on the these laws. Coletti and Macchietto investigated Local fouling rates, a moving deposit boundary and the deposit–flow interaction in a multi-pass shell-and-tube unit [15]; Diaz-Bejarano to an aged and removable multi-component fouling, supporting full cycles of fouling–cleaning which have been used in plant diagnostics and pre-heat-train optimizations since [16]. These models are quite strict; they, however, require determining coupled partial differential equations outside specialized software and their computational weight is frequently a lot of in excess of the keyword regarding the data from the plant plane to drive them. A comparative data-driven approach predicts fouling resistance or deposit thickness through neural, support-vector and related models, while model-based methods deduce fouling from excess thermal and hydraulic loads or include it into predictive control [17], [18], [19], [20]. Such models match their training range well, but are poor at extrapolating and neither provide closed-form sensitivities of duty versus velocity nor temperature.

Thermal methods thus precisely characterize performance at a particular coefficient, asymptotic and threshold laws indicate how the coefficient degrades, distributed models link those two rigorously but at high computational cost in dedicated software, and data-driven models are good fits but offer neither generalization nor sensitivity. Knowledgeable us do not recognize a compact treatment that concurrently gives explicit coupling of the ε–NTU heat field to an asymptotic fouling law with mechanistic velocity and temperature dependence, closed-form sensitivity coefficients for the major execution measures, one dimensionless degradation set, and sufficient computational cost in order for possible online applications without requiring any commercial simulator.

This paper occupies that niche. We derive, entirely from first principles and free of a commercial simulator, a quasi-steady dynamic model in which coupled with an asymptotic Kern–Seaton fouling law are the energy balance, LMTD relation and ε–NTU formulation. Everything is classical, in short; the novelty is in their synthesis being closed, and what that means it makes computable. First, fouling resistance progresses through a single ordinary differential equation where its deposition and removal terms are explicit power laws in tube velocity and an Arrhenius function of film temperature, so flow rate and temperature appear mechanistically, rather than as fitted parameters. Second, at each instant, the thermal field is solved quasi-steadily based on the exact ε–NTU relations; hence, the global coefficient, duty, effectiveness and both outlet temperatures change in a consistent way with respect to the deposit. Third, we derive closed form normalized sensitivity coefficients for the effectiveness, the duty and overall coefficient which rank how strongly each operating variable moves the performance. A fourth finding is that the asymptotic loss of effectiveness and duty collapse on a single dimensionless group, the fouling-degradation number $\Theta = U_c R_f^*$, which acts as a compact design criterion.

The remainder of the paper is organized as follows. Section 2 presents the proposed method, including the physical assumptions, governing equations, fouling model, numerical implementation, and illustrative case study. Section 3 presents the model validation, simulation results, sensitivity and uncertainty analyses, and discussion of the findings in relation to established approaches. Section 4 concludes the study by summarizing the main findings, practical implications, and limitations.

Materials and Methods

Physical picture

We consider a single-phase, two-stream shell-and-tube heat exchanger operated in counterflow, in which a hot process stream is cooled by a colder stream. On the surface separating the two fluids a fouling layer accumulates, adding a thermal resistance in series with the two convective films and the tube wall. The layer grows because material is deposited from the fluid faster than the flow can scour it away; as it thickens, the deposition and removal rates approach one another and the resistance tends to a plateau. This is the asymptotic behavior first rationalized by Kern and Seaton.

Two-time scales are present and they are widely separated. The thermal residence time of the fluids and the time for the temperature field to respond to a disturbance are of the order of seconds to minutes, whereas the fouling layer develops over days to months. This separation is the physical justification for a quasi-steady treatment: on the slow fouling clock, the exchanger is, at every instant, in thermal steady state. We therefore solve the steady ε–NTU relations at each moment for the current value of the fouling resistance, and let that resistance evolve according to a first-order deposition–removal law. The coupling runs in both directions, because the fouling rate depends on the surface (film) temperature, which is itself set by the current thermal state of the exchanger.

Assumptions and their justification

The model rests on the following assumptions. Each is stated with the physical reasoning that supports it and, where relevant, the range over which it holds.

A1 — Quasi-steady thermal field. Because the fouling time constant (tens of days, Section 6) exceeds the thermal response time (minutes) by three to four orders of magnitude, the temperature field equilibrates essentially instantaneously relative to deposit growth. The exchanger is treated as being in thermal steady state at every instant while the fouling resistance advances in time.

A2 — Constant, mean physical properties. Specific heats, densities, viscosities and conductivities are evaluated at the mean bulk temperature of each stream and held constant. For the moderate temperature spans of a single unit this introduces only a small error; strongly temperature-dependent properties would require the step-wise evaluation noted as a limitation in Section 7.

A3 — Uniform overall coefficient at each instant. The overall coefficient is taken as uniform over the surface at any given time (it still varies in time as fouling proceeds). This is the standard premise of both the LMTD and ε–NTU methods and is accurate when the streams are well mixed in cross-section.

A4 — Adiabatic shell and negligible axial effects. Heat loss to the surroundings and axial conduction in the wall and fluids are neglected, consistent with a well-insulated unit operating at a high Péclet number.

A5 — Single-phase, sensible-heat duty. No boiling or condensation occurs; both streams exchange sensible heat only. Two-phase operation is outside the present scope.

A6 — Thin deposit, lumped fouling resistance. The deposit is thin relative to the tube radius (for the case of Section 4 its thickness is of order 0.1 mm against a tube radius of tens of millimeters), so the change in flow area and heat-transfer area is negligible and the deposit can be represented by a single series thermal resistance referred to the reference area.

A7 — Deposition–removal kinetics. Net deposit growth is the difference between a deposition term, taken as an Arrhenius function of film temperature and a power law in velocity (mass-transfer/surface-reaction control), and a removal term proportional to the deposit already present and to a power of velocity (shear scouring). This is the Kern–Seaton form with the temperature and velocity dependences made explicit in the manner of Ebert and Panchal and Yeap.

A8 — Time-invariant kinetic parameters. The deposition and removal pre-factors and the activation energy are constant, i.e. the feed composition does not change over the horizon considered. Feed variability would make these parameters time-dependent (Section 9).

Mathematical Derivations

Steady-flow energy balance

Applying the first law to each stream under steady flow, with no shaft work and no heat loss (A4), the duty transferred equals the enthalpy change of each stream:

$$Q = C_h\,(T_{h,i} - T_{h,o}) \qquad (1)$$

$$Q = C_c\,(T_{c,o} - T_{c,i}) \qquad (2)$$

where the heat-capacity rates are

$$C_h = \dot{m}_h\, c_{p,h}\,, \qquad C_c = \dot{m}_c\, c_{p,c} \qquad (3)$$

Q = heat-transfer rate (duty), W

C_h, C_c = heat-capacity rates of hot and cold streams, W K^{-1}

$\dot{m}_h$, $\dot{m}_c$ = mass flow rates, kg s^{-1}

$c_{p,h}$, $c_{p,c}$ = specific heats, J kg^{-1} K^{-1}

$T_{h,i}$, $T_{h,o}$ = hot-stream inlet and outlet temperatures, K (or °C)

$T_{c,i}$, $T_{c,o}$ = cold-stream inlet and outlet temperatures, K (or °C)

It is convenient to identify the smaller and larger of the two heat-capacity rates and their ratio:

$C_{min} = min(C_h, C_c)$, $C_{max} = max(C_h, C_c)$, $C_r = C_{min}/C_{max}$ (4)

C_r = heat-capacity-rate ratio, dimensionless ($0 \le C_r \le 1$)

Local rate equation and the LMTD

Over a differential element of surface dA the local rate equation is

$dQ = U\,(T_h - T_c)\,dA = U\,\Delta T\,dA$ (5)

U = overall heat-transfer coefficient, W m^{-2} K^{-1}

ΔT = local temperature difference between the streams, K

A = heat-transfer surface area, m^2

Differentiating $\Delta T = T_h - T_c$ along the surface and using the differential forms of Eqs. (1)– (2) for counterflow gives $d(\Delta T) = -dQ\,(1/C_h - 1/C_c)$. Substituting dQ from Eq. (5) yields $d(\Delta T)/\Delta T = -U(1/C_h - 1/C_c)\,dA$, which integrates over the whole surface to $ln(\Delta T_2/\Delta T_1) = -UA(1/C_h - 1/C_c)$. Eliminating the heat-capacity rates with Eqs. (1)– (2), $(1/C_h - 1/C_c) = (\Delta T_1 - \Delta T_2)/Q$, and rearranging gives the LMTD result:

$Q = U\,A\,\Delta T_{lm}$ (6)

$\Delta T_{lm} = (\Delta T_1 - \Delta T_2)/\,ln(\Delta T_1/\Delta T_2)$ (7)

ΔT_{lm} = logarithmic mean temperature difference, K

ΔT_1, ΔT_2 = terminal temperature differences; for counterflow $\Delta T_1 = T_{h,i} - T_{c,o}$ and $\Delta T_2 = T_{h,o} - T_{c,i}$, K

Equation (6) is exact for a constant overall coefficient and constant heat-capacity rates. It is the natural form when all four terminal temperatures are known and the area is required. When an installed exchanger fouls, however, the coefficient falls and the outlet temperatures become unknowns, so the effectiveness–NTU form of Section 3.4 is preferred; the two are algebraically equivalent.

Overall coefficient and the fouling resistance

Adding the series thermal resistances of the two convective films, the tube wall and the fouling deposits, and referring them to the reference (outer) surface, the clean overall coefficient is

$1/U_c = 1/h_h + R_w + 1/h_c$, $R_w = \frac{\delta_w}{K_w}$ (8–9)

U_c = clean overall heat-transfer coefficient, W m^{-2} K^{-1}

h_h, h_c = hot and cold side film coefficients, W m^{-2} K^{-1}

R_w = wall conduction resistance, m^2 K W^{-1}

δ_w, k_w = wall thickness (m) and thermal conductivity (W m^{-1} K^{-1})

Fouling adds a single lumped resistance R_f in series (A6), so the fouled coefficient is

$1/U_f = 1/U_c + R_f \Rightarrow U_f = U_c / (1 + U_c R_f)$ (10–11)

U_f = fouled overall coefficient, W m^{-2} K^{-1}

R_f = fouling (thermal) resistance referred to A, m^2 K W^{-1}

The group $U_f/U_c = 1/(1 + U_c R_f)$ is the cleanliness factor. Equation (11) already shows the essential non-linearity of fouling: because the fouling resistance is added to 1/U rather than to U, the same increment of R_f costs more duty when the clean coefficient is high than when it is low.

Effectiveness–NTU formulation

The thermodynamic maximum duty is that of an infinitely long counterflow exchanger, in which the stream of smaller heat-capacity rate is brought to the inlet temperature of the other stream:

$Q_{max} = C_{min}\,(T_{h,i} - T_{c,i})$ (12)

The effectiveness and the number of transfer units are defined by

$\varepsilon = Q / Q_{max}$, $NTU = U\,A / C_{min}$ (13–14)

ε = thermal effectiveness, dimensionless ($0 \le \varepsilon \le 1$)

NTU = number of transfer units, dimensionless

Starting from the integrated LMTD relation $ln(\Delta T_2/\Delta T_1) = -NTU(1 - C_r)$ and expressing the terminal differences in terms of ε and C_r, the standard counterflow effectiveness relation follows:

$\varepsilon = [1 - exp(-NTU(1 - C_r))] / [1 - C_r\,exp(-NTU(1 - C_r))]$, $C_r < 1$ (15)

$\varepsilon = NTU / (1 + NTU)$, $C_r = 1$ (16)

Once the effectiveness is known, the duty follows from Eq. (13) and the outlet temperatures from the energy balances (1)–(2):

$T_{h,o} = T_{h,i} - Q/C_h\,,\quad T_{c,o} = T_{c,i} + Q/C_c$ (17)

The Eqs. (15)– (17) are the thermal engine of the model. Given the instantaneous overall coefficient $U_f(t)$ from Eq. (11), they return the effectiveness, the duty and both outlet temperatures without iteration. Since NTU is directly proportional to U, any reduction in $U_f(t)$ caused by fouling decreases the heat exchanger effectiveness and, for fixed inlet conditions and heat-capacity rates, results in a corresponding reduction in the heat-transfer duty.

Asymptotic fouling law with velocity and temperature dependence

Following the deposition–removal picture, the net rate of growth of the fouling resistance is

$$\frac{dR_f}{dt} = \varphi_d - \varphi_r \quad (18)$$

φ_d = deposition rate of fouling resistance, m² K W⁻¹ s⁻¹

φ_r = removal rate of fouling resistance, m² K W⁻¹ s⁻¹

Adopting the Kern–Seaton hypothesis that removal is proportional to the amount of deposit present, $\varphi_r = b_r R_f$, while deposition is set by the local conditions, $\varphi_d = a_d$, Eq becomes a linear first-order ordinary differential equation:

$dR_f/dt = a_d - b_r R_f$ (19)

With the clean initial condition $R_f(0) = 0$ the solution is the classical asymptotic curve

$R_f(t) = R_f^* [1 - \exp(-t/\tau)]$ (20)

$R_f^* = a_d / b_r,\quad \tau = 1 / b_r$ (21)

a_d = deposition coefficient, $m^2\,K\,W^{-1}\,s^{-1}$

b_r = removal-rate coefficient, s^{-1}

R_f^* = asymptotic fouling resistance, $m^2\,K\,W^{-1}$

τ = fouling time constant, s

The mechanistic content is placed in the two coefficients. Deposition is taken as an Arrhenius function of the film (deposition-surface) temperature and a power law in the mean velocity, reflecting reaction- or mass-transfer-controlled attachment; removal is taken proportional to the wall shear stress, which for turbulent flow scales approximately as the square of the velocity:

$a_d = A_d\, u^m \exp(-E_a / R_g T_f)$ (22)

$b_r = A_r\, u^n$ (23)

A_d = deposition pre-factor, $m^2\,K\,W^{-1}\,s^{-1}\,(m\,s^{-1})^{-m}$

A_r = removal pre-factor, $s^{-1}\,(m\,s^{-1})^{-n}$

u = mean tube (fouling-side) velocity, $m\,s^{-1}$

m, n = velocity exponents of deposition and removal, dimensionless (here $m \approx 0.4$, $n \approx 2$)

E_a = activation energy of the deposition reaction, $J\,mol^{-1}$

R_g = universal gas constant, 8.314 $J\,mol^{-1}\,K^{-1}$

T_f = film (deposition-surface) temperature, K

Substituting Eqs into Eq gives explicit expressions for the plateau and the time constant:

$R_f^*(u, T_f) = (A_d/A_r)\, u^{m-n} \exp(-E_a / R_g T_f)$ (24)

$\tau(u) = 1 / (A_r\, u^n)$ (25)

For computation it is convenient to normalize Eq to a reference velocity u_0 and reference film temperature $T_{f,ref}$ at which the asymptotic resistance is $R_{f,ref}^*$:

$R_f^*(u, T_f) = R_{f,ref}^*\, (u/u_0)^{m-n} \exp[\,(E_a/R_g)(1/T_{f,ref} - 1/T_f)\,]$ (26)

Film-temperature closure

The fouling law needs the temperature at the deposition surface, which links it back to the thermal state. Splitting the temperature drop across the series resistances, the film temperature on the fouling side is estimated from the current overall coefficient and the fouling-side film coefficient:

$T_f = T_{h,avg} - (U/h_h)(T_{h,avg} - T_{c,avg})$ (27)

$T_{h,avg}$ = arithmetic mean hot-stream temperature, $(T_{h,i}+T_{h,o})/2$, K

$T_{c,avg}$ = arithmetic mean cold-stream temperature, $(T_{c,i}+T_{c,o})/2$, K

As fouling lowers U, the ratio U/h_h falls and T_f rises toward the hot-stream temperature; through the Arrhenius factor of Eq this accelerates further deposition. Equation is the closure that makes temperature an active, coupled variable rather than a fixed parameter.

Coupled quasi-steady algorithm

Equations (11), (13)–(17), (19), (23), (26) and (27) form a closed set. On the slow fouling clock, the thermal relations are algebraic and the only differential equation is Eq for Rf. This implies that we solve a single ODE and follow it with an algebraic thermal update at each step.

1. Evaluate Uf from Eq. (11).
2. Calculate NTU (14), ε (15)–(16), Q (13) and T−outlet from (17).
3. First you will be evaluating the film temperature Tf (27), then Rf*(26) and finally br (23).
4. Form the rate from Eq $dR_f/dt = b_r\,(R_f^* - R_f)$ (19) and advance Rf in time.

For this reason, the method is explicit and requires neither matrix inversion nor iterations of nested loops which renders it cheap enough to be used in repetitions on-line.

The fouling-degradation number

The loss in performance is asymptotic and dominated by a single dimensionless group, the ratio of the clean coefficient to the plateau resistance,

$$\Theta = U_c\, R_f^* \qquad (28)$$

Θ = fouling-degradation number, dimensionless

From Eq. (11) the asymptotic cleanliness factor and the asymptotic NTU ratio are $U_f^*/U_c = NTU_\infty/NTU_c = 1/(1 + \Theta)$. Group Θ is a Biot-like number that compares deposits resistance versus clean holistic resistance, as it collapses the family of degradation curves and gives compact design criterion; targeting intolerable NTU loss directly translates into an upper-bound on Θ.

Closed-form sensitivity coefficients

A key advantage of an analytical model is we can write its sensitivities in closed form. Using the normalized sensitivity $S_x^Y = (x/Y)(\partial Y/\partial x)$, differentiation of Eq. (15) gives, with $\beta = NTU(1 - C_r)$,

$$\partial\varepsilon/\partial NTU = (1 - C_r)^2 \exp(-\beta) \,/\, [1 - C_r \exp(-\beta)]^2 \qquad (29)$$

$$S_{NTU}{}^{\varepsilon} = (NTU/\varepsilon)(\partial\varepsilon/\partial NTU) \qquad (30)$$

The sensitivity of the overall coefficient to the fouling resistance follows from Eq. (11):

$$S_{R_f}{}^{U} = (R_f/U)(\partial U/\partial R_f) = -\,U_c\, R_f \,/\, (1 + U_c\, R_f) = -\Theta/(1+\Theta) \qquad (31)$$

Hence there are two exact identities: because the duty is a function of inlet temperature difference at constant effectiveness, and NTU is proportional to U

$$S_{\Delta Tin}{}^{Q} = 1,\; S_U{}^{Q} = S_{NTU}{}^{\varepsilon} \qquad (32\text{-}33)$$

By application of the chain rule, we obtain the sensitivity of the duty with respect to the flow rate on minimum capacity stream. Since $C_{min} \propto \dot{m}$ and the film coefficient scales as $h_h \propto u^{0.8} \propto \dot{m}^{0.8}$, so that $S_{\dot{m}}{}^{U} = 0.8\, U/h_h$ and $S_{\dot{m}}{}^{NTU} = S_{\dot{m}}{}^{U} - 1$,

$$S_{\dot{m}}{}^{Q} = 1 + S_{NTU}{}^{\varepsilon}(S_{\dot{m}}{}^{U} - 1) \qquad (34)$$

Equation (34) describes a behavior that is genuinely non-intuitive: increased flow rate raises duty (numerator 1), but lowered NTU (the negative term), hence the overall gain is sub-proportional. Section 6.4 lists the corresponding numerical values of all these coefficients for the case study.

Uncertainty propagation

Because the model is analytical, measurement uncertainties propagate to the predicted quantities in closed form. From Eq. (1), $Q = \dot{m}_h\, c_{p,h}(T_{h,i} - T_{h,o})$, the relative uncertainty of the duty is

$$(u_Q/Q)^2 = (u_{\dot{m}}/\dot{m})^2 + (u_{cp}/c_p)^2 + 2\,(u_T/\Delta T_h)^2 \qquad (35)$$

u_Q, $u_{\dot{m}}$, u_{cp}, u_T = standard uncertainties of duty, mass flow, specific heat and temperature

ΔT_h = hot-stream temperature change, $T_{h,i} - T_{h,o}$, K

When the overall coefficient is inferred from measured duty and temperatures through $U = Q/(A\,\Delta T_{lm})$, the fouling resistance obtained from Eq. (10), $R_f = 1/U_f - 1/U_c$, carries an uncertainty

$$u_{Rf} = u_U \,/\, U_f^2 \qquad (36\text{–}37)$$

Equation (35) shows why a close temperature approach is dangerous for monitoring: as ΔT_h

shrinks, the term $2(u_T/\Delta T_h)^2$ grows, and the same absolute temperature error produces a much larger relative error in the inferred duty and, through Eq. (37), in the fouling resistance. This is quantified for the case study in Section 6.5.

Numerical implementation

The model was implemented from scratch in Python 3 using only the NumPy numerical library; no commercial process simulator, computational-fluid-dynamics package or symbolic-algebra tool was used at any stage. The single ordinary differential equation for the fouling resistance Eq was integrated with the classical fourth-order Runge–Kutta scheme using a fixed step of 0.25 day over a 360-day horizon. At every step the thermal update (Section 3.7) was evaluated algebraically, so the whole calculation is explicit and non-iterative. Step-size halving changed the computed asymptotic resistance by less than 0.01%, confirming that the reported results are step-independent. The complete calculation for one operating case runs in well under a second on an ordinary desktop, which is the property that makes the model suitable for embedding in a monitoring or scheduling loop.

Illustrative case study

To exercise the model, we use a counterflow shell-and-tube exchanger in which a hot process stream is cooled by water. However, the operating point and physical properties are characteristic of a light-hydrocarbon cooler; they are internally consistent but illustrative, they were chosen to show the model rather than to reflect a specific measured unit. All derived quantities duty, effectiveness, outlet temperatures, fouling resistance are computed from the governing equations of Section 3 and are therefore thermodynamically consistent with the stated inputs. Figure 1 shows the arrangement and Table 1 lists the input parameters.

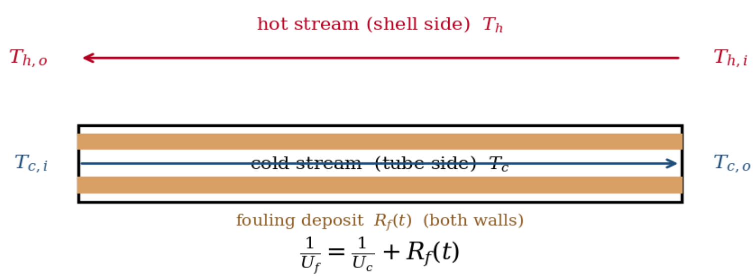

Figure 1. Counterflow shell-and-tube arrangement used in the case study.

The hot stream (shell side) and cold stream (tube side) flow in opposite directions; a fouling deposit of time-dependent resistance $R_f(t)$ grows on the heat-transfer surface and adds in series with the clean resistance, so that $1/U_f = 1/U_c + R_f(t)$.

Table 1. Input parameters of the illustrative counterflow case study (illustrative, thermodynamically consistent).

Parameter	Symbol	Value	Unit
Heat-transfer area	A	80	m^2
Hot-stream mass flow	$\dot{m}_h$	12	$kg\ s^{-1}$
Hot-stream specific heat	$c_{p,h}$	2200	$J\ kg^{-1}\ K^{-1}$
Cold-stream mass flow	$\dot{m}_c$	20	$kg\ s^{-1}$
Cold-stream specific heat	$c_{p,c}$	4180	$J\ kg^{-1}\ K^{-1}$
Hot inlet temperature	$T_{h,i}$	180	°C
Cold inlet temperature	$T_{c,i}$	25	°C
Hot-side film coefficient (at u_0)	h_h	700	$W\ m^{-2}\ K^{-1}$
Cold-side film coefficient	h_c	1500	$W\ m^{-2}\ K^{-1}$
Wall resistance	R_w	6.0×10^{-5}	$m^2\ K\ W^{-1}$
Reference tube velocity	u_0	1.5	$m\ s^{-1}$
Reference asymptotic resistance	$R_{f,ref}^*$	4.0×10^{-4}	$m^2\ K\ W^{-1}$
Removal pre-factor	A_r	1.715×10^{-7}	$s^{-1}\ (m\ s^{-1})^{-2}$
Deposition velocity exponent	m	0.4	–
Removal velocity exponent	n	2.0	–
Activation-energy group	E_a/R_g	3000	K

Clean design point

Evaluating Eqs gives C_h = 26.4 kW K^{-1} and C_c = 83.6 kW K^{-1}, so the hot stream carries the minimum heat-capacity rate, C_{min} = 26.4 kW K^{-1}, and C_r = 0.316. With the clean coefficient U_c = 464 W m^{-2} K^{-1} from Eqs, the clean design point follows from Eqs and is summarized in Table 2. These values are the baseline against which the fouled states of Section 6 are measured.

Table 2. Calculation of clean design point result based on equations.

Quantity	Symbol	Clean value
Minimum heat-capacity rate	C_{min}	26.4 kW K^{-1}
Heat-capacity-rate ratio	C_r	0.316
Clean overall coefficient	U_c	464 W m^{-2} K^{-1}
Number of transfer units	NTU	1.406
Effectiveness	ε	0.703
Duty	Q	2875 kW
Hot outlet temperature	$T_{h,o}$	71.1 °C
Cold outlet temperature	$T_{c,o}$	59.4 °C
Reference film temperature	$T_{f,ref}$	70.3 °C

Results

Since the case-study data are not measured, but rather illustrative, validation in this context is showing that the implementation produces analytical limits consistent with self-consistent governing equations and qualitative trends identified through the literature of experiments. Three independent checks are reported.

Consistency of the ε–NTU and LMTD routes

Since the energy balance and local rate equation generate both ε–NTU and LMTD methods must return the same duty for identical conditions. The effectiveness was then computed using the following eq. The outlet temperatures to form one logarithmic-mean temperature difference and separate duty U A ΔT_{lm}. As can be seen in Figure 2(a), the LMTD cross-check points meet the ε -NTU curve perfectly over the full range, verifying both their algebraic equivalence as well as implementation correctness.

Verification of the fouling law

However, Eq. Exact solution of Eq. (19) is scenario in which the force homogeneously distributed along y direction 20). In Figure 2(b), the true trajectory, which evolves according to Eq. The frozen-temperature closed-form, The two curves have identical initial slope and time constant; they diverge only as the increasing temperature of the rising film in the coupled solution raises the plateau, just the positive feedback found in Section 3.5. The agreement in the early, temperature-independent regime confirms the integrator and controlled divergence at late times verifies that the temperature coupling functions as designed.

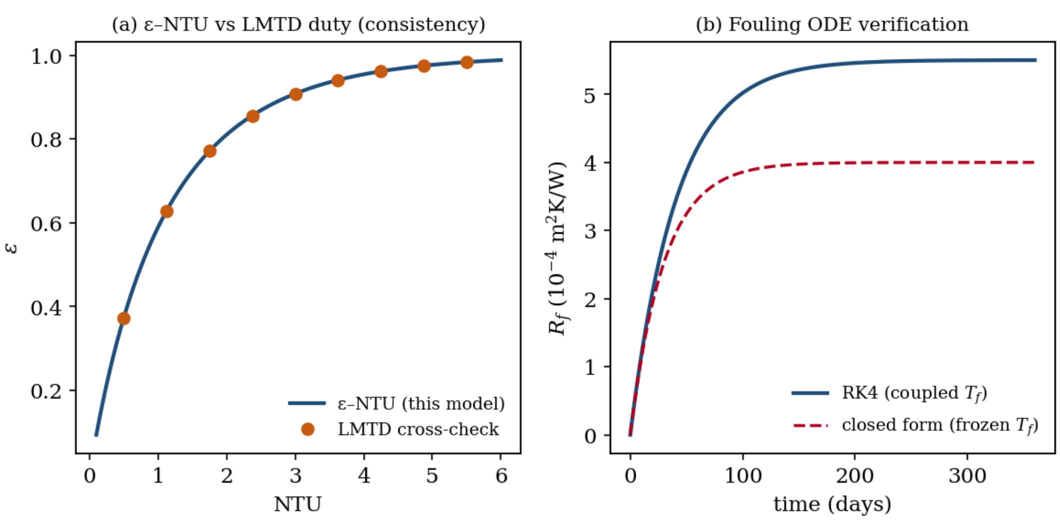

Figure 2. Model verification.

(a) Effectiveness from the ε–NTU relation (line) and duty recomputed using the LMTD route (points); however, they are equal along this NTU range. (b) The tal in fouling resistance from the coupled Runge-Kutta solution (solid) and frozen-film-temperature closed form of Eq (dashed'; they agree at short times and diverge only when the coupled film temperature increases the plateau.

Consistency with experimental trends

The model produces the main qualitative trends observed experimentally for fouling systems, beyond internal validation. In the first one, the decrease of asymptotic resistance is monotonic with an increase in speed (Eq. 24 with m < n) which conform with long-standing observation that enhanced shear suppresses net deposition. Second, for n = 2 (removal exponent) the fouling time constant scales as u^{-2}, this trend matching the inverse-square reliance of time fouling on velocity that was previously reported for both water-side and crude-oil systems. Third, the Arrhenius dependence of the plateau on film temperature reproduces the accelerating effect of surface temperature that underlies the threshold behavior of Ebert and Panchal. The quantitative demonstration of these trends is given in Section 6.2 and 6.3. Finally, the energy balance is satisfied identically at every instant by construction, since the duty entering the cold stream equals that leaving the hot stream in Eqs.

Dynamic performance degradation at the design velocity

Integrating the coupled model at the design velocity produces the fouling trajectory of Figure 3 and the performance degradation of Figure 4. The fouling resistance rises from zero and approaches an asymptote of $R_f^* = 5.50 \times 10^{-4}$ m^2 K W^{-1} with a time constant of about 30 days; roughly three-time constants (three months) are needed before the deposit is effectively fully developed. The corresponding fouling-degradation number is $\Theta = U_c R_f^* = 0.255$.

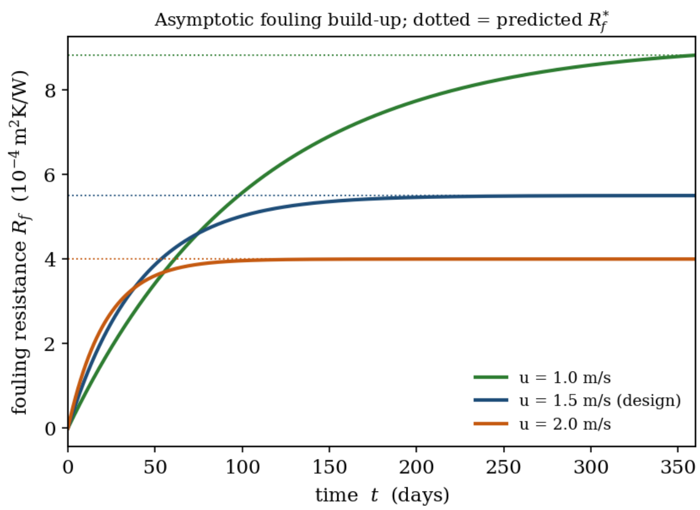

Figure 3. Asymptotic build-up of fouling resistance for three tube velocities.

Solid curves are the computed trajectories; dotted lines mark the predicted asymptotes R_f^*. Higher velocity lowers the plateau and shortens the time constant simultaneously.

The consequences for performance are shown in Figure 4 and tabulated month by month in Table 3. Over the horizon the overall coefficient falls by 20.3% (from 464 to 370 W m^{-2} K^{-1}), yet the effectiveness and the duty fall by only 10.7% (the duty from 2875 to 2567 kW). One of the most useful outputs of the model is this asymmetry. It occurs because the exchanger functions on the concave section of the ε–NTU curve: where effectiveness responds in less than sub-proportion to NTU; elasticity ${S_{NTU}}^{\varepsilon} = 0.463$ (Section 7.4), so a loss of NTU by 20% results in a duty drop attenuated by ~11%. For instance, an engineer who assumed that the fractional loss of coefficient is equal to the fractional loss in duty would be writing a thermal penalty almost two times too high.

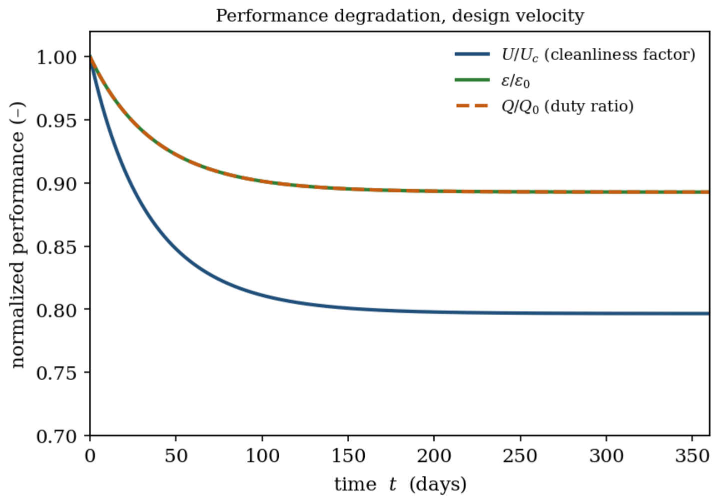

Figure 4. Performance at design velocity

Normalized the cleanliness factor U/U_c decreases faster compared to $\varepsilon/\varepsilon_0$ and Q/Q_0 because of the nature of exchanger operation on the concave part of the ε–NTU curve. A coefficient of this magnitude results in only an 11% reduction in duty, despite being a 20% drop.

Table 3. The predicted monthly performance at the design velocity (u = 1.5 m s^{-1}).

Time (months)	R_f (10^{-4} m^2K/W)	U (W/m^2K)	NTU	E	Q (kW)	$T_{h,o}$ (°C)	$T_{c,o}$ (°C)
0 (clean)	0.00	464.0	1.406	0.703	2875	71.1	59.4
1	2.85	409.9	1.242	0.662	2708	77.4	57.4
2	4.22	388.0	1.176	0.644	2634	80.3	56.5
3	4.89	378.2	1.146	0.635	2599	81.6	56.1
6	5.43	370.6	1.123	0.628	2571	82.6	55.8
9	5.50	369.7	1.120	0.627	2568	82.8	55.7
12	5.50	369.6	1.120	0.627	2567	82.8	55.7

The outlet temperatures show in Table 3 and Figure 5 indicate the operational details without interpretation: as the exchanger fouls, the hot stream leaves hotter (71.1 → 82.8 °C), and the cold stream cooler (59.4 → 55.7 °C) due to a decreasing amount of heat exchanged between the two streams. In a pre-heat train this hotter hot-outlet is precisely the signature that downstream furnaces must make up, and it is directly observable, which is what makes the model useful as a soft sensor.

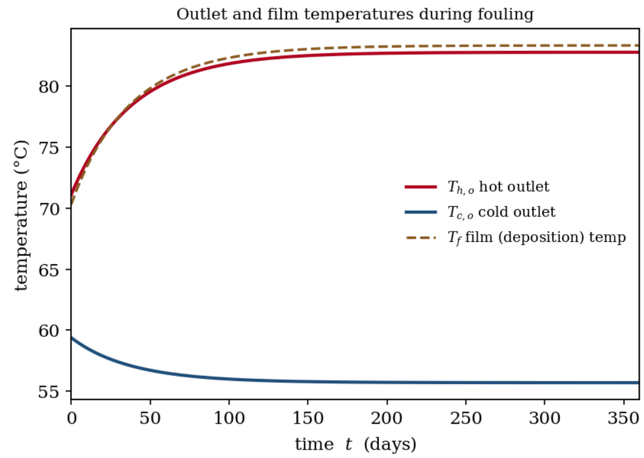

Figure 5. Evolution of the outlet and film temperatures during fouling at the design velocity.

As duty is lost the hot outlet rises and the cold outlet falls; the film (deposition-surface) temperature rises, which feeds back through the Arrhenius term to accelerate early deposition.

Effect of flow rate

Figure 3 also contains the three velocity cases, and the contrast is the clearest single demonstration of why a condition-dependent model is needed. Raising the velocity from 1.0 to 2.0 m s^{-1} lowers the asymptotic resistance from 8.83×10^{-4} to 4.00×10^{-4} m^2 K W^{-1} and shortens the time constant from 67.5 to 16.9 days. The plateau follows the predicted $u^{m-n} = u^{-1.6}$ law and the time constant the predicted u^{-2} law. A fixed fouling factor would assign all three cases the same resistance and would therefore misrepresent both the severity and the speed of fouling by more than a factor of two. The result is also revealing a real design trade-off: while more velocity mitigates fouling, pumping power increases approximately with the (cube) of velocity, so this requires a punch in at least one axis end model appropriate for exploring an optimum balance.

Effect of temperature

Figure 6 isolates the two dependences of the asymptotic resistance. The left panel confirms the monotonic decrease of R_f^* with velocity; the right panel shows the Arrhenius increase with film temperature, R_f^* roughly tripling as the film temperature rises from 120 to 190 °C. Because the film temperature is not an independent input but is set by the thermal state through Eq, and because it rises as the deposit grows, the model captures the self-accelerating character of high-temperature fouling without any additional assumption. This is the mechanism behind the threshold behavior of chemical-reaction fouling and is the reason that, in practice, the hottest exchangers in a train foul the fastest.

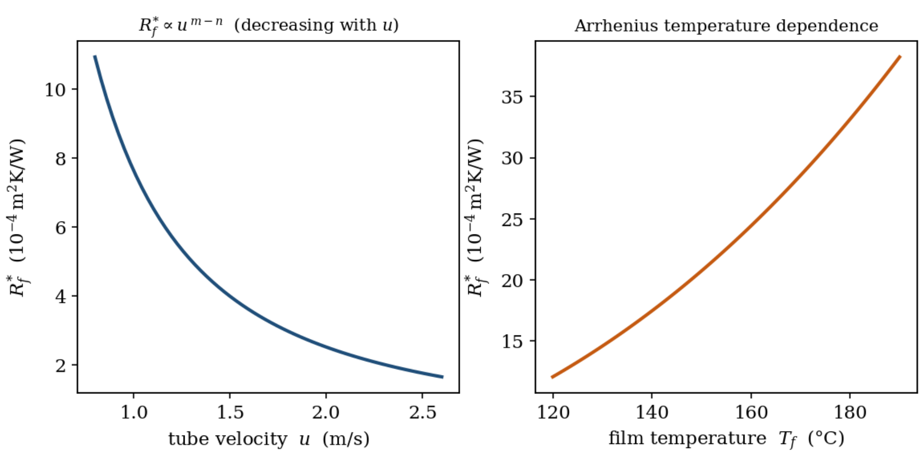

Figure 6. Parametric dependence of the asymptotic fouling resistance.

Left: R_f^* decreases with tube velocity as u^{m-n}. Right: R_f^* increases with film temperature through the Arrhenius factor of Eq. (26). The two panels quantify the competing shear and reaction effects.

Operating-point shift and sensitivity ranking

Figure 7 places the clean and fully fouled states on the counterflow ε–NTU chart. Fouling moves the operating point down and to the left along the C_r = 0.316 contour, from (NTU = 1.41, ε = 0.70) to (NTU = 1.12, ε = 0.63). The near-horizontal spacing of the contours in this region is the graphical statement of the attenuation discussed in Section 6.1.

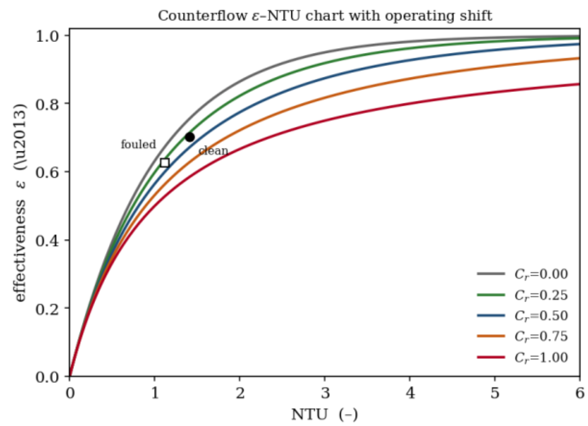

Figure 7. Counterflow ε–NTU chart with the operating-point shift caused by fouling.

The filled circle is the clean state and the open square the fully fouled state; fouling slides the point down the C_r = 0.316 contour. The flatness of the contour at this NTU is why an appreciable loss of NTU produces a smaller loss of effectiveness.

In Figure 8, and Table 4 we collect the normalized sensitivity coefficients of Section 3.9 evaluated for the case study. Their ranking is directly actionable. Duty is the most sensitive to (S = 1.000, a perfect proportionality) inlet temperature difference, so any drift in hot supply temperature maps 1: 1 onto duty. Flow rate is next (S = 0.706): increasing the minimum-stream flow raises duty, but sub-proportionally, because it simultaneously depresses NTU, the competition made explicit in Eq. The duty responds to the overall coefficient with the same elasticity as the effectiveness responds to NTU (S = 0.463), a consequence of the exact identity of Eq. Finally, the coefficient's sensitivity to fouling, $S_{Rf}^{U} = -\Theta/(1+\Theta) = -0.203$ at the design asymptote, quantifies how strongly deposition erodes the coefficient and shows that this erosion is itself throttled by the $1/(1+\Theta)$ factor.

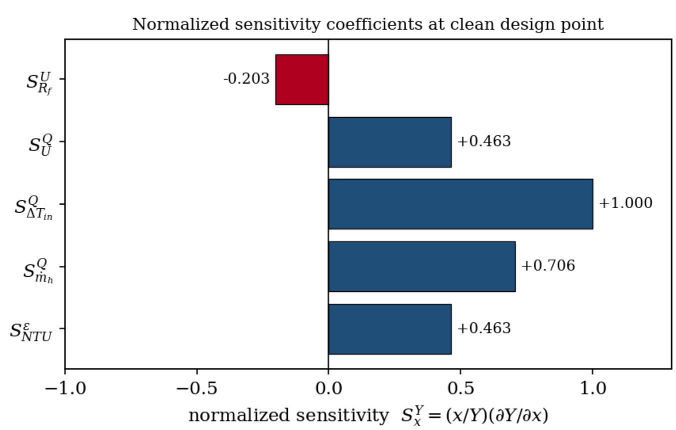

Figure 8. Normalized sensitivity coefficients at the design point (the fouling sensitivity is evaluated at the design-velocity asymptote).

Positive bars increase the response variable; the duty is governed most strongly by the inlet temperature difference, then by flow rate, then by the overall coefficient.

Table 4. Closed-form normalized sensitivity coefficients evaluated for the case study.

Coefficient	Meaning	Value	Interpretation
S_{NTU}^{ε}	effectiveness vs NTU	+0.463	sub-proportional; concave region
$S_{\dot{m}}^{Q}$	duty vs min-stream flow	+0.706	gain offset by NTU loss
$S_{\Delta T_{in}}^{Q}$	duty vs inlet ΔT	+1.000	exact proportionality
S_{U}^{Q}	duty vs overall coeff.	+0.463	equals S_{NTU}^{ε} (Eq. 33)
$S_{R_f}^{U}$	coeff. vs fouling	−0.203	$= -\Theta/(1+\Theta)$

Uncertainty analysis
Applying Eqs. (35)–(37) with representative instrument uncertainties 2% on each mass flow, 1% on each specific heat and ±0.5 K on each temperature gives a relative uncertainty of 2.3% in the computed duty and 2.9% in the inferred overall coefficient. Propagated through Eq. (37), the standard uncertainty in the asymptotic fouling resistance is 0.97×10^{-4} m^2 K W^{-1}, which is about 18% of the resistance itself. Table 5 summarizes these figures.

Table 5. Illustrative uncertainty budget (measurement uncertainties: 2% flow, 1% specific heat, ±0.5 K temperature).

Quantity	Nominal value	Relative/ absolute uncertainty
Duty, Q	2875 kW	±2.3%
Overall coefficient, U	464 W m^{-2} K^{-1}	±2.9%
Asymptotic fouling resistance, R_f^*	5.50×10^{-4} m^2 K W^{-1}	$\pm 0.97 \times 10^{-4}$ (≈ 18%)

The disproportionate uncertainty in the inferred fouling resistance is not a defect of the model but a warning that the model makes quantitative. Equation (35) shows that the temperature term is amplified by $1/\Delta T_h$, so an exchanger with a small hot-side temperature changes a close temperature approach will yield a poorly determined fouling resistance from the same instruments. The practical recommendation is that fouling monitoring based on inferred resistance should be treated with appropriate caution on units operating near their temperature pinch, and that the temperature instrumentation on such units repays particular attention.

Discussion

Against the fixed fouling factor. The industrial standard remains a constant fouling allowance added once at design. The present model contains that practice as a degenerate special case setting R_f to a constant recovers the fixed-factor result but replaces the constant with a resistance that evolves in time and depends mechanistically on velocity and film temperature. The velocity study of Section 6.2, in which the asymptotic resistance varies by more than a factor of two across a realistic velocity range, shows concretely what the fixed factor discards.

Against threshold models. The number of surfaces is mechanistically dependent on surface shear and temperature in Ebert and Panchal threshold framework, but it is expressed as a deposition term minus a constant shear-removal term (constant rate below the threshold leading to non-plateauing rates), consistent with the present model. The present model instead follows Kern and Seaton in making removal proportional to the deposit, which yields an asymptotic plateau. The two are complementary: the threshold form is the right description when the design objective is to stay in a no-fouling regime, whereas the asymptotic form is the right description when a stable fouling layer is expected and the question is how much performance is ultimately lost. A practical model could switch between them; here the asymptotic form was chosen because a plateau is the more common industrial observation and because it yields the compact degradation number Θ.

Against distributed dynamic models. The distributed, first-principles models of Coletti and Macchietto and Diaz-Bejarano resolve the axial variation of fouling, the ageing of the deposit and the two-way coupling with the hydraulics through a moving-boundary formulation, and are the appropriate tools when spatial and compositional detail is required. That fidelity is bought with the numerical solution of coupled partial differential equations and, in practice, dedicated software. The present model is deliberately lumped: it sacrifices axial resolution and deposit ageing in exchange for an analytical, simulator-free formulation whose entire state is a single scalar and whose sensitivities are available in closed form. The two occupy different points on the fidelity cost frontier, and are complementary rather than competing a lumped model of this kind is a natural reduced-order companion to a distributed model, and a natural core for a lightweight digital twin.

Against data-driven models. Machine-learning predictors of fouling resistance can achieve excellent accuracy within the envelope of their training data, and hybrid monitoring schemes infer foulant behavior from excess loads or embed fouling in advanced control. Their weaknesses are the mirror image of the present model's strengths: they extrapolate unreliably and offer no analytical sensitivity. Conversely, the present model does not learn from data automatically; its kinetic parameters must be fitted. The most promising route is hybrid using the mechanistic model as a physics-informed backbone whose few parameters are estimated from data which is noted in Section 9.

Against transient ε–NTU treatments. Time-dependent ε–NTU formulations have been developed for fast transients such as inlet step changes and mass discharge. The present work applies the ε–NTU framework on the opposite, slow time scale of fouling, where the quasi-steady approximation is rigorously justified by the separation of time scales, and couples it to a deposition–removal law rather than to a thermal-inertia term.

Strengths

Transparency and reproducibility. Every relation is derived in closed form and every parameter has a physical meaning and an SI unit; another researcher can reproduce the model from Section 3 alone.

Analytical sensitivity. The closed-form coefficients of Eqs give a directly interpretable ranking of design and operating levers that a black-box model cannot provide.

A single degradation group. The number $\Theta = U_c R_f^*$ collapses the asymptotic loss and converts a performance target into an explicit ceiling on the deposit resistance.

Computational economy and independence. A single scalar ODE with algebraic updates runs in well under a second and needs no commercial simulator, making the model suitable for on-line monitoring and for scanning many operating or design scenarios.

Honest uncertainty. The analytical error propagation exposes, rather than hides, the amplification of measurement error near a close temperature approach.

Limitations

Lumped in space. A single film temperature and a single fouling resistance represent the whole surface; the axial rise of wall temperature, and therefore the axial variation of fouling, is not resolved. For long units with strong temperature gradients a distributed treatment is preferable.

Constant properties and single phase. Strongly temperature-dependent properties and any boiling or condensation are outside the present scope and would require a step-wise or two-phase extension.

No hydraulic coupling or ageing. The model tracks the thermal resistance of the deposit but not its effect on pressure drop, nor the change of its properties as it ages; both are known to matter in crude-oil service.
Asymptotic form only. The Kern–Seaton closure assumes a plateau; systems showing linear, falling-rate or long induction-period behavior would need a different rate law, although the coupling framework would be unchanged.
Parameters require calibration. The deposition and removal pre-factors and the activation energy must be fitted to plant or laboratory data before quantitative prediction on a specific unit; the case study demonstrates the structure, not calibrated constants for a named fluid.
Counterflow idealization. The usual LMTD correction factor or the proper ε–NTU relation would result in multi-pass and cross-flow arrangements; pure counterflow is considered here only.

Industrial applications

Three applications follow directly from the structure of the model. First, as a soft sensor: from continuously measured flows and terminal temperatures Eqs ensure that an inferred overall coefficient and fouling resistance are continually calculated in real time with the uncertainty of Section 6.5 attached; supplying a physically grounded fouling-monitoring signal. Second, as a cleaning-schedule and screening tool: because the model is cheap and analytical, the degradation trajectory can be extrapolated forward at any combinations of velocity or feed temperature to determine when the accumulated duty loss warrants a clean, while also providing Θ as a one-line comparison metric for ranking possible operating points. Third, as a design aid: the explicit velocity and temperature dependences let the designer choose a velocity that keeps Θ below a target while weighing the cubic pumping-power penalty, rather than relying on a table value that is blind to both. In each case the model's value is not that it is the most accurate description available, but that it is transparent, differentiable and fast enough to be used routinely.

Conclusion

A compact, simulator-independent mathematical model of heat-exchanger performance under fouling has been developed from first principles by coupling the steady-flow energy balance, the LMTD relation and the effectiveness–NTU formulation to an asymptotic Kern–Seaton fouling law whose deposition and removal terms are explicit functions of tube velocity and film temperature. The following conclusions are drawn.

The performance of a fouling exchanger can be described completely by integrating a single scalar ordinary differential equation for the fouling resistance while solving the exact ε–NTU relations quasi-steadily at each instant, with no recourse to any commercial process simulator.

For the illustrative counterflow case, a 20.3% loss of overall coefficient produced only a 10.7% loss of duty, because the exchanger operates on the concave part of the ε–NTU curve. The model quantifies this attenuation by means of the elasticity ${S_{NTU}}^{\varepsilon} = 0.463$ and alerts against confusing coefficient loss with duty loss.

The asymptotic fouling resistance and the fouling time constant scale as u^{m-n} and u^{-2} respectively, causing the plateau and its approach to be highly velocity-dependent; a fixed fouling factor will therefore yield errors greater than a factor of two in predicting resistance over any reasonable range of velocities.

The asymptotic performance loss is combined into a single dimensionless group, fouling-degradation number $\Theta = U_c R_f^*$, that serves as a specific upper limit on the deposit resistance translated from duty target.

Closed-form normalized sensitivity coefficients rank the operating levers uniquely: scaled duty is directly proportional to the inlet temperature difference, sub-proportional with respect to flow rate and responds to overall coefficient as effectiveness responds to NTU, both having the same elasticity.

We demonstrate through analytical uncertainty propagation that the fouling resistance derived from measured duty has approximately 18% uncertainty for the stated instrumentation, and that this uncertainty is magnified for units operating close to a tight temperature approach a practically important caveat for fouling monitoring.

References

[1] F. Coletti and S. Macchietto, “Dynamic, distributed model of shell-and-tube heat exchangers undergoing crude oil fouling,” Ind. Eng. Chem. Res., vol. 50, no. 8, pp. 4515–4533, 2011, doi: 10.1021/ie901991g.

[2] F. Lozano-Santamaria and S. Macchietto, “Assessment of a dynamic model for the optimization of refinery preheat trains under fouling,” Heat Transfer Engineering, vol. 43, nos. 15–16, pp. 1349–1364, 2022, doi: 10.1080/01457632.2021.1963537.

[3] Tubular Exchanger Manufacturers Association, Standards of the Tubular Exchanger Manufacturers Association, 9th ed. TEMA, 2007.

[4] N. Epstein, “Thinking about heat transfer fouling: A 5 × 5 matrix,” Heat Transfer Engineering, vol. 4, no. 1, pp. 43–56, 1983, doi: 10.1080/01457638108939594.

[5] B. L. Yeap, D. I. Wilson, G. T. Polley, and S. J. Pugh, “Mitigation of crude oil refinery heat exchanger fouling through retrofits based on thermo-hydraulic fouling models,” Chem. Eng. Res. Des., vol. 82, no. 1, pp. 53–71, 2004, doi: 10.1205/026387604772803070.

[6] R. K. Shah and D. P. Sekulić, Fundamentals of Heat Exchanger Design. Hoboken, NJ, USA: John Wiley & Sons, 2003.

[7] S. Kakaç, H. Liu, and A. Pramuanjaroenkij, Heat Exchangers: Selection, Rating, and Thermal Design, 4th ed. Boca Raton, FL, USA: CRC Press, 2020, doi: 10.1201/9780429469862.

[8] T. L. Bergman, A. S. Lavine, F. P. Incropera, and D. P. DeWitt, Fundamentals of Heat and Mass Transfer, 8th ed. Hoboken, NJ, USA: John Wiley & Sons, 2018.

[9] J. Yin and M. K. Jensen, “Analytic model for transient heat exchanger response,” Int. J. Heat Mass Transfer, vol. 46, no. 17, pp. 3255–3264, 2003, doi: 10.1016/S0017-9310(03)00118-2.

[10] P. Regulagadda, G. F. Naterer, and I. Dincer, “Time varying NTU method for heat exchanger analysis with mass discharge,” Heat Mass Transfer, vol. 48, no. 10, pp. 1763–1771, 2012, doi: 10.1007/s00231-011-0914-5.

[11] D. Q. Kern and R. E. Seaton, “A theoretical analysis of thermal surface fouling,” British Chemical Engineering, vol. 4, no. 5, pp. 258–262, 1959.

[12] M. Čarnogurská, M. Příhoda, M. Andrejiová, and L. Tóth, “Analysis of the mathematical models for identifying the thickness of the fouling layer in natural gas coolers,” Applied Sciences, vol. 14, no. 10, Art. no. 4003, 2024, doi: 10.3390/app14104003.

[13] W. A. Ebert and C. B. Panchal, “Analysis of Exxon crude-oil slip-stream coking data,” in Fouling Mitigation of Industrial Heat Exchange Equipment, C. B. Panchal, T. R. Bott, E. F. C. Somerscales, and S. Toyama, Eds. New York, NY, USA: Begell House, 1997, pp. 451–460.

[14] D. I. Wilson, E. M. Ishiyama, and G. T. Polley, “Twenty years of Ebert and Panchal—What next?” Heat Transfer Engineering, vol. 38, nos. 7–8, pp. 669–680, 2017, doi: 10.1080/01457632.2016.1206407.

[15] F. Coletti, S. Macchietto, and G. T. Polley, “Effects of fouling on performance of retrofitted heat exchanger networks: A thermo-hydraulic based analysis,” Comput. Chem. Eng., vol. 35, no. 5, pp. 907–917, 2011, doi: 10.1016/j.compchemeng.2011.01.027.

[16] E. Diaz-Bejarano, F. Coletti, and S. Macchietto, “A new dynamic model of crude oil fouling deposits and its application to the simulation of fouling-cleaning cycles,” AIChE J., vol. 62, no. 1, pp. 90–107, 2016, doi: 10.1002/aic.15036.

[17] P. Patil, B. Srinivasan, and R. Srinivasan, “A simple model-based methodology to characterize foulants in heat exchangers using excess thermal and hydraulic loads,” Chem. Eng. Res. Des., vol. 185, pp. 326–343, 2022, doi: 10.1016/j.cherd.2022.07.011.

[18] A. Zaza, E. G. Bennouna, A. Iranzo, Y. El Hammami, and F. J. Pino, "Optimizing sustainability in hybrid cooling towers: Investigating fouling resistance, water quality correlations, modeling, and cleaning strategies for thermal power plants," J. Cleaner Prod., vol. 462, Art. no. 142706, 2024, doi: 10.1016/j.jclepro.2024.142706.
[19] P. K. Resma Madhu and J. Subbaiah, "Iterative quality weighted interpolation for LPV-MPC control of industrial heat exchanger under varying fouling conditions," Asia-Pacific Journal of Chemical Engineering, vol. 17, no. 5, Art. no. e2811, 2022, doi: 10.1002/apj.2811.
[20] V. C. Aiello, G. Kini, M. A. Staedter, and S. V. Garimella, "Investigation of fouling mechanisms for diesel engine exhaust heat recovery," Applied Thermal Engineering, vol. 181, Art. no. 115973, 2020, doi: 10.1016/j.applthermaleng.2020.115973.